THE ASTRONOMICAL JOURNAL VOLUME 92, NUMBER 5 NOVEMBER 1986

COLOR GRADIENTS IN THREE VIRGO ELLIPTICALS

JUDITH G. COHEN
Palomar Observatory, California Institute of Technology, Pasadena, California 91125
Received 29 April 1986; revised 1 August 1986

ABSTRACT

Accurate surface photometry at optical wavelengths is presented for NGC 4486, NGC 4472, and NGC 4406. Ellipses of varying ellipticity and position angle as a function of semimajor axis (A) are fit over the range in A spanned by the data, $2 \leqslant A \leqslant \approx 400$ arcsec. Color gradients in these galaxies are definitely present but are quite small. For each galaxy, the parameters describing the fit ellipses in the four colors are identical.

I. INTRODUCTION

The development of digital area detectors with high quantum efficiency and low-noise characteristics has made it possible to carry out investigations of surface photometry of galaxies of unprecedented precision. The limiting factor in such studies is generally the small size of the detector. We describe here an analysis of the photometric properties of three luminous Virgo ellipticals using a new instrument with a mosaic of four CCD chips to enable larger spatial coverage. In Sec. II we describe the observational material, while Sec. III details the analysis of the two-dimensional images. The results of our work are outlined in Sec. IV, where the deduced color gradients and properties of the ellipses fit to each galaxy are examined. A brief summary is contained in Sec. V.

II. OBSERVATIONS

Three of the brightest elliptical galaxies in the core of the Virgo cluster (NGC 4486, NGC 4472, and NGC 4406) have been observed with the 4-Shooter (Gunn *et al.* 1984) on the 200 in. Hale telescope in March 1985. The field of the 4-Shooter is a square approximately 9 arcmin on a side, with a scale of 0.33 arcsec/pixel. Many 800 s exposures through the g filter of the Thuan-Gunn system (Thuan and Gunn 1976) were obtained for each galaxy, and at least one long exposure in the r filter and in the i filter of this system is also available. Several of the long g and r frames from the nights of 15 and 16 March 1985, which were photometric and had seeing better than 1.3 arcsec, were used in this study. The long exposures through the i filter of NGC 4472 and NGC 4406 were taken on a nonphotometric night, while that of NGC 4486 was taken on 16 March 1985. There is also a single frame of each galaxy taken through the v (violet) filter, as well as short exposures in the g, r, and i filters, although these were taken on a nonphotometric night of somewhat poorer seeing. For the nuclear regions, we obtained short exposures taken on 29 May 1986 (a photometric night with seeing better than 1.2 arcsec) using a single CCD chip at the Cassegrain focus of the 60 in. telescope at Palomar Observatory. No additional optics beyond the primary and secondary mirror of the telescope, the filter, and the Dewar window were present; the scale was 0.47 arcsec/pixel.

III. ANALYSIS

a) Ellipse Fitting on the 4-Shooter Frames

After the frames were flattened, ellipses were fit using a program based originally on the algorithms of P. J. Young described in Kent (1983), but specially modified to reject the numerous point sources (i.e., the globular clusters). The center of the galaxy was fixed at a location chosen by inspection of each frame when displayed on a suitable monitor. No iterations for the center of the profile were allowed. Elliptical isophotes were fit over the range of the semimajor axis (A) from 8 arcsec to the maximum achievable in steps of 0.02 in the logarithm of A. The position of the nucleus of each galaxy was always at a fixed location in the frame, but the maximum semimajor axis reached ranges from 366 to 420 arcsec depending on where the nucleus of the galaxy was placed and on the ellipticity of the galaxy. An effort was made to force the bright star about 50 arcsec west of the nucleus of NGC 4472 to fall on the apex of the 4-Shooter pyramid (thus falling through the approximately 1 arcsec crack between the chips). This helped reduce the perturbation of adjacent areas of the frame. The nucleus of NGC 4472 was thus located east of the center of the frame. NGC 4406 was also offset from the center of the frame to produce a good determination of the background sky.

Two special circumstances occurred. For NGC 4486, it was necessary to mask out the jet in the inner part of the galaxy ($A \leqslant 35$ arcsec). In this case a cone 40° wide centered on the position angle of the jet was omitted from the fitting procedure. Although Ford and Butcher (1979) present evidence for the presence of ionized gaseous filaments in and near the nucleus of NGC 4486, we avoid the nucleus itself, and the filaments beyond 8 arcsec radius are so faint that they do not noticeably perturb the isophotes. The second problem arises from the square-frame format and, in two cases, the noncentral galaxy placement. The range of position angle within the frame at large values of A becomes much less than the full 360° coverage, and the solution for the position angle and ellipticity, ϵ, where $\epsilon = 1 - b/a$ of the fit ellipse, then becomes quite uncertain. In practice, for $A \geqslant 250$ arcsec, ϵ and the position angle were fixed at the mean of the five points with A between 210 and 250 arcsec.

Several regions always gave problems and are omitted from the final fits. These include the region near the bright star west of the nucleus of NGC 4472 ($A \approx 63$ arcsec) and the region of the dwarf galaxy near the nucleus of NGC 4406 ($A \approx 7$ arcsec).

b) Sky Determination

The count levels achieved in these frames are such that in the long exposures the sky was about 2300 data numbers/pixel (henceforth referred to as dn) (which corresponds to about 4600 electrons/pixel) in the g filter, 1700 dn in the r filter, and 7500 dn in the i filter, while the nuclei of the galaxies were grossly saturated. The sky level was determined by

 0004-6256/86/051039-09$00.90

examining the statistical properties of the frames in the corners of the field farthest from the galaxy center. Fits were carried out down to a level of about 5% of the sky and g and r. The sky brightness was typically 21.8 mag arcsec^{-2} in g and 21.2 mag arcsec^{-2} in the r filter. The sky in the near-infrared i filter is significantly brighter. There is no doubt that for NGC 4406 the background sky has been reached in the appropriate corners of the frames. The sky level in all the short exposures is also well determined. A larger format detector would, however, be useful for NGC 4486 and for NGC 4472 to ensure that the sky level is reached. Lacking such, we used the observed sky brightness in each color in our frames and the photoelectric drift scans through the corona of NGC 4486 by de Vaucouleurs and Nieto (1978) to deduce that in the corners of the 4-Shooter frames, the halo of NGC 4486 contributes about 2% of the "apparent sky" in g and in r, and about 1% in the i bandpass, where the sky is significantly brighter. The apparent sky was therefore lowered by 2% in g and in r and by 1% in i for NGC 4486 and NGC 4472. The sky in g and r on the frames of NGC 4486 and NGC 4472 cannot be overestimated by more than 4%, otherwise it would be noticeably darker than was measured on the frames of NGC 4406, which were interleaved among the frames of the two brighter galaxies. One should also note that because these galaxies and the sky have roughly comparable colors, modifying the adopted background level in this way affects the $(g-r)$ or $(r-i)$ colors by less than 0.01 mag for $A \leqslant 100$ arcsec and by less than 0.02 mag for $A \leqslant 200$ arcsec. The surface brightness in g at $A = 200$ arcsec is brighter by 0.12 mag in NGC 4486 when the sky is reduced by 2%, and the change in g surface brightness for NGC 4472 at the same semimajor axis is only 0.08 mag.

An additional uncertainty in the fitting is the accuracy of flat fielding of the data and the necessity of transferring this information across the four-chip format. The straightforward flat-fielding algorithm used here relies on illumination of a painted spot on the dome by a light source mounted at the top of the prime-focus cage of the telescope. Tests indicate that the accuracy of this process is significantly better locally within a frame than globally between chips or across large parts of chips. An accuracy of 1.0% is the limit achievable without a significantly more sophisticated flat-field algorithm, such as has been developed by Schmidt, Schneider, and Gunn (1986).

Saturation of the analog-to-digital electronics occurs at 32 767 dn, and full-well depth of the CCD is somewhat larger. The ellipse fits were halted at $A_{\rm lim}$, where intensities exceeded 25 000 dn. This occurred at $A_{\rm lim} \approx 25$ arcsec in NGC 4486 and in NGC 4472 for the 800 s g frames. However, it was clear that the central regions of the long-exposure frames, even at levels which naively were safely below chip saturation, were being affected by charge bleeding from the heavily saturated galaxy nuclei or by light scattered from the nuclei of the galaxies by optics within the 4-Shooter. Tests on the image of a very bright star on a night of good seeing show that in the direction in which charge bleeding should not be significant (i.e., along a row of the CCD) scattering with its r^{-2} intensity falloff becomes equal to the (approximately) Gaussian seeing profile about 5 arcsec away for the point source, at which point the intensity is 1.0×10^{-3} of that in the central pixel. Beyond 5 arcsec, the intensity profile of a point source falls off roughly as r^{-2}.

Rather than attempt to remove the effects of scattering by deconvolutions, I instead choose to patch the long and short exposures together at a much larger radius than the minimum $A_{\rm lim}$. The actual locations for the patch were chosen by inspecting the magnitude gradients in the short- and long-exposure frames in the large region of overlap. The semimajor axis at the patching locations ($A_{\rm p}$) used was about 70 arcsec in NGC 4486 and in NGC 4472, and about 45 arcsec in the somewhat fainter galaxy NGC 4406. The color gradients taken from the short exposures on nonphotometric nights were patched onto those from the long exposures using the region of overlap near $A_{\rm p}$.

No corrections were made for the very small variations in scale introduced by the use of transmission elements in the optical path. These scale differences (in the form of pixels/arcsec), relative to that of the g filter, are 0.9966, 1.0044, and 1.0055 for the v, r, and i filters, respectively. Beyond using a larger value of $A_{\rm p}$ than the minimum, as described above, no corrections for scattering in the optics were made.

c) The Nuclear Region

The single-chip CCD frames taken with the Palomar 60 in. telescope were used for the region $2 \leqslant A \leqslant 8$ arcsec only. For NGC 4486, the isophotes were assumed to be round over that interval in A. No allowance for the jet was made, as the contrast between the bright nucleus and the relatively faint jet is large. The ellipse parameters fit for the region just beyond $A = 8$ arcsec were used for the inner region of the two other galaxies. Fits were carried out in 1 pixel steps, rather than in uniform increments of log (A). The sky level was always well determined on these frames and the nuclei of the galaxies were never saturated. Since the minimum number of optical surfaces was used, scattered light is also not a problem.

d) Photometric Transformations

Standard stars were observed on the photometric nights. A transformation to the standard photoelectric Thuan-Gunn system was made for the g and r observations (as well as the i data of NGC 4486 only). The i data for NGC 4472 and NGC 4406 have been transformed from the instrumental system to the photoelectric one via the transformations derived on photometric nights, and are only missing the correct zero point. Small uncertainties in zero point of less than 0.05 mag still exist in the final colors, but do not enter when colors at different locations within the same galaxy are compared. These uncertainties arise primarily because most of the standard stars observed on each night are significantly bluer than the galaxies. Note that the $v-g$ colors are given on the instrumental (ins) system. Analysis of data for standard stars obtained on photometric nights indicates that, although the blue sensitivity of the CCD detectors is low, the v filter bandpass is narrow and well defined, and the transformation between the 4-Shooter instrumental and photoelectric $v-g$ color is given by $(v-g)_{\rm pe} = 0.962\ (v-g)_{\rm ins} + A - B \sec(z)$, where A and B are constants and z is the zenith angle.

IV. RESULTS

a) Ellipse Parameters

The final parameters for the three galaxies are listed in Tables I–V. The first two tables list the parameters of the ellipse fits for NGC 4406, NGC 4472, and NGC 4486, respectively. The first column of each section of Table I gives

TABLE I. Ellipticities for NGC 4406, 4472, and 4486.

A arc-sec	ϵ(g)	$\delta\epsilon$(g,r)	$\delta\epsilon$(g,i)	$\delta\epsilon$(g,v)	ϵ(g)	$\delta\epsilon$(g,r)	$\delta\epsilon$(g,i)	$\delta\epsilon$(g,v)	ϵ(g)	$\delta\epsilon$(g,r)	$\delta\epsilon$(g,i)	$\delta\epsilon$(g,v)
		NGC 4406				NGC 4472				NGC 4486		
8.1	0.13	0.00	−0.01	0.02	0.07	−0.02	−0.03	−0.02	0.02	0.00	−0.01	0.00
8.8	0.13	0.00	−0.01	0.01	0.09	0.00	−0.01	−0.01	0.01	0.00	0.00	−0.01
9.7	0.14	0.00	−0.01	0.00	0.09	−0.01	−0.01	−0.01	0.02	0.00	0.00	0.00
10.6	0.14	−0.01	−0.02	0.00	0.10	−0.01	−0.01	−0.01	0.02	0.00	0.00	0.00
11.6	0.15	−0.01	−0.01	0.00	0.11	0.00	−0.01	0.00	0.02	0.00	0.00	0.00
12.8	0.15	−0.02	−0.01	−0.01	0.12	0.00	−0.01	0.00	0.03	0.00	0.00	0.00
14.0	0.16	−0.02	−0.01	−0.01	0.13	0.00	−0.01	−0.01	0.03	−0.01	0.00	0.00
15.3	0.17	0.00	0.00	0.01	0.14	0.00	−0.01	0.00	0.03	0.00	0.00	0.00
16.8	0.17	−0.01	−0.01	−0.01	0.15	0.00	−0.01	0.00	0.04	0.00	0.00	0.00
18.5	0.19	0.00	0.00	0.01	0.16	0.00	0.00	0.00	0.04	0.00	0.00	0.00
20.2	0.19	0.00	0.00	0.00	0.16	0.00	0.00	0.01	0.04	0.00	0.00	0.00
22.2	0.19	−0.01	−0.01	−0.01	0.16	0.00	0.00	0.00	0.04	0.00	0.00	−0.01
24.3	0.20	0.00	0.00	0.00	0.16	0.00	0.00	0.00	0.05	0.01	0.00	0.00
26.7	0.21	−0.01	−0.01	0.00	0.17	0.00	0.00	0.00	0.05	0.00	0.00	−0.01
29.2	0.22	0.00	0.00	0.01	0.16	0.00	0.00	0.00	0.05	0.00	0.00	−0.01
32.1	0.23	0.00	0.00	0.00	0.16	0.00	0.00	0.00	0.05	0.00	0.00	0.00
35.2	0.24	−0.01	−0.01	−0.01	0.15	0.00	0.00	0.00	0.06	0.00	0.00	0.00
38.5	0.26	0.01	0.01	0.00	0.16	0.00	0.00	0.01	0.07	0.00	0.00	0.00
42.3	0.25	−0.02	−0.04	0.00	0.15	0.00	0.00	0.01	0.07	0.00	0.00	0.00
46.3	0.25	−0.02	−0.03	0.01	0.15	0.00	−0.01	0.01	0.07	0.00	0.00	0.00
50.8	0.25	−0.01	−0.03	0.00	0.14	−0.01	−0.01	0.01	0.08	0.00	0.00	0.00
55.7	0.26	−0.01	−0.02	0.01	0.14	−0.01	0.00	0.00	0.08	0.00	0.00	0.00
60.8	0.26	−0.01	−0.01	−0.01					0.09	0.00	0.00	0.00
66.7	0.27	0.00	0.00						0.10	0.00	0.00	0.00
70.1					0.17	0.00	0.00	0.01				
76.6					0.21	0.01	−0.01		0.11	0.00	0.00	0.00
83.9	0.26	−0.02	−0.01		0.20	0.02	−0.01		0.13	−0.01	−0.02	
92.0	0.25	−0.02	−0.01		0.20	0.00	−0.01		0.14	−0.01	−0.02	
100.9	0.26	−0.02	−0.02		0.19	0.00	−0.01		0.14	−0.01	−0.01	
110.7	0.25	−0.03	−0.02		0.18	−0.01	−0.02		0.14	−0.01	−0.01	
121.3	0.24	−0.03	−0.02		0.18	−0.01	−0.01		0.16	−0.01	0.00	
133.0	0.24	−0.03	−0.02		0.17	−0.01	−0.01		0.16	−0.01	0.00	
145.9	0.25	−0.03	−0.02		0.17	−0.01	−0.01		0.18	−0.01	0.00	
160.0	0.27	−0.03	−0.01		0.18	−0.01	−0.01		0.19	−0.01	0.00	
175.4	0.30	−0.04	−0.01		0.18	−0.02	−0.01		0.20	−0.02	0.00	
192.3	0.31	−0.05	−0.01		0.19	−0.02	−0.01		0.21	−0.03	−0.01	
210.9	0.31	−0.05	−0.02		0.20	−0.03	−0.02		0.22	−0.03	−0.02	
231.2	0.29	−0.06	−0.03		0.21	−0.04	−0.02		0.23	−0.04	−0.04	

the semimajor axis (A) in arcsec, followed by the ellipticity determined from the g frames. The differences in ϵ deduced from frames in the various colors as compared to that of the g frame are given in the next three columns. Table II lists the position angle (P.A.) determined in the g frame as a function of semimajor axis, and the differences between the position angle as determined from images through the other filters. Tables III–V give the photometric results, in particular the surface brightness per arcsec^2 in each filter. For each filter, we define a maximum and minimum value based on a $\pm$ 1.5% uncertainty in the sky level. The adopted uncertainties in the background sky level for NGC 4406 were + 1% and − 2% of the sky. This leads to g_{max} and g_{min} at each semimajor axis. The worst-case combination of the resulting errors between the two filters defining any color leads to similar maximum and minimum values of the color. The first column of each table lists the semimajor axis, while the subsequent columns give the g magnitude, g_{max}, g_{min}, the $g-r$ color, $(g-r)_{max}$, $(g-r)_{min}$, the $r-i$ color, $(r-i)_{max}$, $(r-i)_{min}$, the $v-g$ color, $(v-g)_{max}$, and $(v-g)_{min}$. (Note that the $v-g$ color is on an instrumental system and has not been transformed to the standard Thuan-Gunn photometric system, although the transformation equation is given above.)

The position angles and ellipticities as a function of semimajor axis derived for the three Virgo ellipticals agree well with those of King (1978). The position angle in the inner 20 arcsec of NGC 4486 is poorly determined since the galaxy is

TABLE II. Position angles for NGC 4406, 4472, and 4486.

A arc-sec	PA(g) °	δPA (g,r)°	δPA (g,i)°	δPA (g,v)°	PA(g) °	δPA (g,r)°	δPA (g,i)°	δPA (g,v)°	PA(g) °	δPA (g,r)°	δPA (g,i)°	δPA (g,v)°
		NGC 4406				NGC 4472				NGC 4486		
8.1	124.0	1.9	4.1	0.9	162.5	2.0	2.4	3.5	173.3	−3.4	0.0	10.0
8.8	123.1	1.7	4.1	1.7	162.7	0.0	2.1	2.8	159.7	−1.9	9.1	2.8
9.7	122.5	2.4	4.2	3.3	160.4	2.2	1.1	0.7	174.4	9.0	2.2	12.5
10.6	120.8	1.3	0.4	0.4	160.1	−0.2	0.6	1.5	156.1	−13.3	−2.7	26.2
11.6	121.4	1.0	1.0	0.6	160.3	1.1	0.3	0.3	158.5	−2.8	−7.9	−2.6
12.8	120.0	0.9	0.0	−0.9	160.2	0.3	0.8	1.6	165.5	0.0	−2.7	10.8
14.0	120.6	1.1	1.2	0.6	159.8	0.4	0.0	0.5	162.0	−6.5	−7.3	2.1
15.3	120.1	0.7	0.2	1.5	160.1	2.1	0.3	0.3	165.4	−5.3	−1.6	7.8
16.8	120.5	0.6	0.0	0.0	159.7	0.4	0.5	−0.6	166.7	−2.5	−1.5	4.4
18.5	118.9	−1.2	−1.6	−1.7	160.5	1.4	0.4	1.0	165.1	−2.7	0.0	2.2
20.2	121.7	1.7	0.8	1.7	160.0	0.6	0.8	0.6	164.2	−1.1	1.5	0.4
22.2	121.8	0.8	1.3	0.8	159.7	0.3	0.3	−0.6	166.6	4.9	3.2	4.4
24.3	122.1	1.1	0.9	1.7	159.7	0.2	0.1	−0.2	161.7	0.3	0.9	0.8
26.7	122.5	1.0	1.0	0.6	159.0	−0.4	−0.3	−0.3	159.4	−1.2	−1.6	−1.9
29.2	122.7	0.2	0.5	1.0	159.0	0.3	0.3	−0.7	160.1	2.3	−0.2	0.2
32.1	122.4	−0.3	0.0	0.1	159.6	0.4	0.7	1.1	158.5	1.0	0.0	−6.3
35.2	121.4	−0.2	−1.0	1.2	159.2	0.3	0.6	0.8	158.8	1.8	0.7	−3.1
38.5	120.2	−1.3	−2.1	−0.2	158.9	0.0	0.4	0.6	160.6	1.7	1.9	0.0
42.3	134.3	3.1	−1.4	−0.4	158.5	0.6	0.2	0.9	158.2	1.2	0.4	−2.1
46.3	133.7	2.8	−0.6	−0.3	157.3	0.2	−0.2	0.8	157.4	0.2	0.4	−1.6
50.8	132.8	2.4	−0.5	0.7	155.1	−0.5	−1.0	1.0	157.2	0.9	0.7	2.3
55.7	132.2	1.6	−0.4	−0.6	152.6	−2.3	0.4	−0.3	158.0	1.2	1.0	−5.9
60.8	132.3	1.5	−0.5	−0.4					154.4	0.5	−1.5	−3.4
66.7	132.6	1.1	−1.0						155.4	0.3	0.2	−1.0
70.1					156.5	1.2	0.2	−0.1				
76.6					154.0	−4.0	3.8		154.7	0.2	−2.2	0.3
83.9	125.4	−1.1	−1.8		152.3	−1.8	1.2		152.0	1.8	1.7	
92.0	122.5	−1.4	−2.5		153.1	1.3	1.6		152.3	1.1	0.9	
100.9	121.1	−1.1	−2.6		154.3	1.6	2.5		153.1	0.9	0.6	
110.7	120.0	−1.2	−1.8		155.1	1.9	2.7		154.0	1.2	0.4	
121.3	118.0	−1.5	−2.3		155.3	2.3	3.6		154.1	1.7	0.3	
133.0	117.5	−1.3	−1.6		155.0	2.2	3.1		153.8	1.7	0.1	
145.9	117.0	−2.0	−1.9		155.0	2.6	3.3		154.3	2.2	−0.5	
160.0	117.5	−1.3	−1.1		155.0	2.7	3.6		155.7	2.0	0.1	
175.4	118.2	−1.4	−1.2		155.0	2.8	3.4		155.9	2.2	−0.7	
192.3	118.8	−1.4	−1.4		154.2	2.3	3.3		157.7	3.6	−0.8	
210.9	120.2	−1.2	−1.8		154.7	2.8	3.2		157.3	2.9	−2.6	
231.2	123.4	1.2	0.2		155.3	3.3	3.2		158.2	2.2	−3.3	

TABLE III. Colors for NGC 4406.

A arc-sec	g mag	δ(g)+ mag	δ(g)− mag	(g-r) mag	δ(g-r)+ mag	δ(g-r)− mag	(g-i) mag	δ(g-i)+ mag	δ(g-i)− mag	(v-g) mag	δ(v-g)+ mag	δ(v-g)− mag
2.3	16.896	0.001	−0.001				0.109	0.002	−0.002			
3.8	17.454	0.002	−0.002				0.107	0.002	−0.002			
5.3	17.859	0.002	−0.002				0.104	0.003	−0.003			
6.8	18.161	0.003	−0.003				0.100	0.004	−0.004			
8.1	18.381	0.011	−0.011	0.495	0.013	−0.013	0.099	0.003	−0.003	0.098	0.019	−0.019
8.8	18.497	0.012	−0.012	0.496	0.015	−0.015	0.104	0.004	−0.004	0.096	0.021	−0.021
9.7	18.604	0.013	−0.013	0.492	0.016	−0.016	0.099	0.004	−0.004	0.094	0.023	−0.023
10.6	18.732	0.015	−0.015	0.499	0.018	−0.018	0.108	0.005	−0.005	0.085	0.026	−0.026
11.6	18.850	0.017	−0.017	0.505	0.021	−0.020	0.107	0.005	−0.005	0.081	0.029	−0.029
12.8	18.970	0.018	−0.019	0.507	0.023	−0.023	0.104	0.006	−0.006	0.073	0.032	−0.032
14.0	19.095	0.021	−0.021	0.510	0.026	−0.025	0.115	0.006	−0.007	0.071	0.036	−0.036
15.3	19.201	0.023	−0.023	0.494	0.029	−0.028	0.099	0.007	−0.007	0.091	0.040	−0.041
16.8	19.336	0.026	−0.026	0.503	0.032	−0.032	0.107	0.008	−0.008	0.073	0.045	−0.046
18.5	19.445	0.028	−0.029	0.486	0.036	−0.035	0.088	0.009	−0.009	0.093	0.050	−0.051
20.2	19.588	0.032	−0.033	0.502	0.041	−0.040	0.103	0.010	−0.010	0.071	0.057	−0.057
22.2	19.717	0.036	−0.038	0.505	0.046	−0.045	0.106	0.012	−0.012	0.073	0.064	−0.065
24.3	19.834	0.041	−0.042	0.493	0.051	−0.050	0.094	0.013	−0.013	0.084	0.072	−0.073
26.7	19.952	0.045	−0.047	0.494	0.057	−0.055	0.092	0.015	−0.015	0.087	0.080	−0.081
29.2	20.063	0.050	−0.052	0.489	0.064	−0.061	0.086	0.016	−0.016	0.084	0.089	−0.090
32.1	20.181	0.055	−0.058	0.489	0.071	−0.068	0.083	0.018	−0.018	0.090	0.099	−0.100
35.2	20.295	0.061	−0.065	0.487	0.079	−0.076	0.080	0.020	−0.020	0.066	0.109	−0.110
38.5	20.400	0.067	−0.072	0.467	0.088	−0.084	0.060	0.023	−0.023	0.103	0.122	−0.124
40.4	20.472	0.072	−0.077	0.465	0.094	−0.089	0.062	0.024	−0.024	0.091	0.129	−0.132
44.1	20.624	0.006	−0.003	0.471	0.012	−0.011	0.068	0.011	−0.011	0.107	0.151	−0.154
48.3	20.771	0.007	−0.004	0.467	0.014	−0.012	0.068	0.012	−0.012	0.125	0.172	−0.176
53.0	20.918	0.008	−0.004	0.460	0.016	−0.014	0.056	0.014	−0.014	0.116	0.196	−0.201
58.1	21.072	0.009	−0.005	0.458	0.018	−0.016	0.048	0.017	−0.016	0.143	0.224	−0.230
63.7	21.236	0.011	−0.005	0.466	0.021	−0.019	0.043	0.019	−0.019	0.122	0.265	−0.273
69.8	21.395	0.013	−0.006	0.459	0.024	−0.022	0.031	0.022	−0.022			
83.9	21.693	0.016	−0.008	0.461	0.032	−0.029	0.028	0.030	−0.029			
92.0	21.848	0.019	−0.010	0.459	0.037	−0.034	0.022	0.034	−0.033			
100.9	22.006	0.022	−0.011	0.470	0.042	−0.039	0.029	0.039	−0.038			
110.7	22.181	0.026	−0.013	0.472	0.050	−0.045	0.024	0.046	−0.045			
121.3	22.371	0.031	−0.016	0.471	0.059	−0.054	0.019	0.055	−0.054			
133.0	22.563	0.036	−0.019	0.471	0.070	−0.064	0.003	0.067	−0.064			
145.9	22.737	0.042	−0.022	0.479	0.082	−0.075	−0.007	0.078	−0.076			
160.0	22.869	0.048	−0.025	0.479	0.092	−0.085	−0.029	0.090	−0.086			
175.4	23.000	0.054	−0.028	0.487	0.103	−0.095	−0.034	0.101	−0.097			
192.3	23.146	0.061	−0.032	0.491	0.118	−0.109	−0.050	0.117	−0.111			
210.9	23.313	0.071	−0.037	0.504	0.136	−0.126	−0.053	0.136	−0.129			
231.2	23.544	0.087	−0.046	0.564	0.161	−0.152	−0.014	0.161	−0.152			
253.5	23.624	0.094	−0.050	0.447	0.186	−0.171	−0.144	0.193	−0.182			
278.0	23.841	0.114	−0.062	0.448	0.225	−0.209	−0.144	0.234	−0.222			
304.8	24.113	0.144	−0.080	0.461	0.284	−0.266	−0.161	0.299	−0.285			
334.2	24.361	0.178	−0.102	0.431	0.359	−0.338	−0.265	0.399	−0.382			
366.4	24.560	0.211	−0.124	0.364	0.443	−0.418	−0.391	0.519	−0.505			
401.8	24.900	0.282	−0.174	0.183	0.653	−0.632	−0.616	0.819	−0.862			

TABLE IV. Colors for NGC 4472.

A arc-sec	g mag	δ(g)+ mag	δ(g)− mag	(g-r) mag	δ(g-r)+ mag	δ(g-r)− mag	(g-i) mag	δ(g-i)+ mag	δ(g-i)− mag	(v-g) mag	δ(v-g)+ mag	δ(v-g)− mag
2.2	16.667	0.001	−0.001				0.155	0.002	−0.002			
3.7	17.008	0.001	−0.001				0.152	0.003	−0.003			
5.1	17.319	0.002	−0.002				0.144	0.003	−0.003			
6.6	17.590	0.002	−0.002				0.138	0.004	−0.004			
8.1	17.829	0.002	−0.002	0.498	0.004	−0.004	0.138	0.003	−0.003	0.709	0.006	−0.006
8.8	17.917	0.003	−0.003	0.492	0.005	−0.005	0.127	0.003	−0.003	0.717	0.006	−0.006
9.7	18.052	0.003	−0.003	0.496	0.005	−0.005	0.129	0.003	−0.003	0.713	0.007	−0.007
10.6	18.158	0.003	−0.003	0.495	0.006	−0.006	0.128	0.004	−0.004	0.710	0.008	−0.008
11.6	18.270	0.003	−0.003	0.488	0.006	−0.006	0.122	0.004	−0.004	0.710	0.009	−0.009
12.8	18.387	0.004	−0.004	0.488	0.007	−0.007	0.125	0.005	−0.005	0.705	0.010	−0.010
14.0	18.506	0.004	−0.004	0.493	0.008	−0.008	0.129	0.005	−0.005	0.696	0.011	−0.011
15.3	18.622	0.005	−0.005	0.491	0.009	−0.009	0.128	0.006	−0.006	0.697	0.012	−0.012
16.8	18.738	0.005	−0.005	0.486	0.010	−0.010	0.127	0.006	−0.006	0.700	0.013	−0.013
18.5	18.860	0.006	−0.006	0.481	0.011	−0.011	0.119	0.007	−0.007	0.698	0.015	−0.015
20.2	18.987	0.007	−0.007	0.488	0.012	−0.012	0.125	0.008	−0.008	0.692	0.017	−0.017
22.2	19.014	0.008	−0.008	0.481	0.014	−0.014	0.121	0.009	−0.009	0.683	0.019	−0.019
24.3	19.247	0.008	−0.009	0.486	0.016	−0.016	0.122	0.010	−0.010	0.680	0.021	−0.021
26.7	19.388	0.010	−0.010	0.480	0.018	−0.018	0.115	0.012	−0.012	0.671	0.024	−0.024
29.2	19.544	0.011	−0.011	0.489	0.021	−0.021	0.124	0.013	−0.013	0.662	0.028	−0.028
32.1	19.702	0.013	−0.013	0.490	0.024	−0.024	0.125	0.015	−0.015	0.647	0.032	−0.032
35.2	19.864	0.015	−0.015	0.491	0.028	−0.028	0.125	0.018	−0.018	0.644	0.037	−0.037
38.5	20.018	0.017	−0.017	0.494	0.032	−0.032	0.117	0.021	−0.021	0.649	0.043	−0.042
42.3	20.179	0.020	−0.020	0.484	0.037	−0.037	0.118	0.024	−0.024	0.635	0.049	−0.049
46.3	20.337	0.023	−0.024	0.486	0.043	−0.043	0.118	0.028	−0.028	0.619	0.056	−0.056
50.8	20.489	0.026	−0.027	0.482	0.050	−0.049	0.110	0.032	−0.032	0.608	0.065	−0.064
55.7	20.642	0.030	−0.031	0.502	0.057	−0.056	0.127	0.037	−0.036	0.585	0.073	−0.073
58.3	20.715	0.032	−0.033	0.509	0.060	−0.060	0.125	0.039	−0.039	0.577	0.078	−0.077
69.8	20.976	0.008	−0.008	0.518	0.015	−0.015	0.120	0.016	−0.016			
76.6	21.101	0.008	−0.009	0.495	0.017	−0.017	0.114	0.019	−0.019			
83.9	21.256	0.010	−0.010	0.487	0.020	−0.020	0.103	0.022	−0.022			
92.0	21.418	0.011	−0.011	0.523	0.023	−0.023	0.107	0.025	−0.025			
100.9	21.592	0.013	−0.013	0.522	0.027	−0.027	0.101	0.029	−0.029			
110.7	21.788	0.016	−0.016	0.530	0.032	−0.032	0.106	0.035	−0.035			
121.3	21.993	0.019	−0.019	0.533	0.039	−0.038	0.102	0.042	−0.043			
133.0	22.206	0.023	−0.024	0.529	0.047	−0.047	0.094	0.051	−0.052			
145.9	22.419	0.028	−0.029	0.534	0.057	−0.057	0.089	0.062	−0.064			
160.0	22.620	0.034	−0.035	0.535	0.069	−0.068	0.078	0.076	−0.078			
175.4	22.811	0.040	−0.042	0.546	0.081	−0.081	0.073	0.090	−0.093			
192.3	22.988	0.047	−0.049	0.550	0.096	−0.095	0.068	0.106	−0.110			
210.9	23.159	0.055	−0.058	0.554	0.112	−0.111	0.069	0.123	−0.129			
231.2	23.336	0.064	−0.068	0.571	0.131	−0.130	0.082	0.143	−0.151			
253.5	23.539	0.077	−0.083	0.565	0.159	−0.157	0.076	0.172	−0.184			
278.0	23.726	0.091	−0.099	0.575	0.188	−0.186	0.060	0.206	−0.223			
304.8	23.925	0.109	−0.121	0.565	0.227	−0.224	0.016	0.253	−0.281			
334.2	24.247	0.143	−0.165	0.620	0.300	−0.293	−0.049	0.346	−0.411			
366.4	24.655	0.202	−0.249	0.721	0.426	−0.406	0.178	0.419	−0.502			
401.8	25.465	0.386	−0.604	0.971	0.898	−0.751	0.640	0.613	−0.745			

TABLE V. Colors for NGC 4486.

A arc-sec	g mag	δ(g)+ mag	δ(g)− mag	(g-r) mag	δ(g-r)+ mag	δ(g-r)− mag	(g-i) mag	δ(g-i)+ mag	δ(g-i)− mag	(v-g) mag	δ(v-g)+ mag	δ(v-g)− mag
2.1	17.380	0.002	−0.002				0.919	0.003	−0.003			
3.5	17.555	0.002	−0.002				0.920	0.003	−0.003			
4.9	17.718	0.002	−0.002				0.920	0.003	−0.003			
6.4	17.880	0.002	−0.002				0.919	0.003	−0.003			
8.0	18.082	0.002	−0.002	0.540	0.004	−0.004	0.925	0.003	−0.003	0.414	0.008	−0.008
8.8	18.168	0.002	−0.002	0.541	0.004	−0.004	0.923	0.004	−0.004	0.409	0.008	−0.008
9.6	18.279	0.002	−0.002	0.541	0.005	−0.005	0.924	0.004	−0.004	0.404	0.009	−0.009
10.6	18.382	0.002	−0.002	0.552	0.005	−0.005	0.918	0.004	−0.004	0.403	0.010	−0.010
11.6	18.489	0.002	−0.002	0.553	0.006	−0.006	0.914	0.005	−0.005	0.407	0.011	−0.011
12.7	18.600	0.003	−0.003	0.556	0.006	−0.006	0.920	0.005	−0.005	0.397	0.012	−0.012
13.9	18.719	0.003	−0.003	0.552	0.007	−0.007	0.914	0.006	−0.006	0.393	0.013	−0.013
15.3	18.842	0.003	−0.003	0.549	0.008	−0.008	0.914	0.007	−0.007	0.388	0.015	−0.014
16.7	18.967	0.004	−0.004	0.548	0.009	−0.009	0.913	0.008	−0.008	0.385	0.016	−0.016
18.4	19.096	0.004	−0.004	0.546	0.010	−0.010	0.911	0.009	−0.009	0.383	0.018	−0.018
20.1	19.231	0.005	−0.005	0.543	0.011	−0.011	0.907	0.010	−0.010	0.382	0.021	−0.021
22.1	19.369	0.005	−0.005	0.540	0.013	−0.013	0.906	0.011	−0.011	0.367	0.023	−0.023
24.2	19.510	0.006	−0.006	0.540	0.014	−0.014	0.905	0.013	−0.013	0.369	0.027	−0.026
26.5	19.654	0.007	−0.007	0.539	0.016	−0.016	0.904	0.015	−0.015	0.359	0.030	−0.030
29.1	19.803	0.008	−0.008	0.537	0.019	−0.019	0.901	0.017	−0.017	0.354	0.035	−0.034
31.9	19.952	0.009	−0.009	0.540	0.022	−0.022	0.900	0.019	−0.019	0.355	0.040	−0.039
35.0	20.101	0.011	−0.011	0.533	0.025	−0.025	0.906	0.022	−0.022	0.351	0.046	−0.045
38.4	20.247	0.012	−0.012	0.532	0.029	−0.029	0.893	0.025	−0.025	0.346	0.052	−0.051
42.1	20.400	0.014	−0.014	0.532	0.033	−0.033	0.903	0.029	−0.029	0.329	0.059	−0.058
46.1	20.553	0.016	−0.016	0.528	0.038	−0.038	0.894	0.034	−0.034	0.330	0.068	−0.066
50.6	20.709	0.019	−0.019	0.529	0.044	−0.044	0.894	0.039	−0.039	0.332	0.079	−0.076
55.5	20.859	0.021	−0.022	0.526	0.050	−0.050	0.891	0.045	−0.045	0.324	0.091	−0.087
60.8	21.016	0.025	−0.025	0.525	0.058	−0.058	0.888	0.052	−0.052	0.321	0.105	−0.100
66.7	21.164	0.028	−0.029	0.522	0.067	−0.067	0.885	0.060	−0.060	0.306	0.120	−0.113
73.1	21.320	0.032	−0.033	0.516	0.077	−0.078	0.884	0.069	−0.069	0.290	0.137	−0.129
80.2	21.499	0.012	−0.012	0.518	0.024	−0.024	0.882	0.027	−0.027			
87.9	21.681	0.014	−0.015	0.524	0.029	−0.029	0.877	0.032	−0.032			
96.4	21.875	0.017	−0.017	0.529	0.034	−0.034	0.881	0.038	−0.038			
105.7	22.074	0.021	−0.021	0.529	0.041	−0.041	0.875	0.046	−0.046			
115.9	22.282	0.025	−0.025	0.535	0.050	−0.050	0.880	0.055	−0.056			
127.1	22.497	0.030	−0.031	0.542	0.061	−0.060	0.874	0.067	−0.069			
139.3	22.719	0.037	−0.038	0.553	0.074	−0.074	0.882	0.081	−0.084			
152.8	22.932	0.045	−0.047	0.564	0.090	−0.089	0.885	0.098	−0.102			
167.5	23.153	0.054	−0.057	0.580	0.109	−0.109	0.897	0.119	−0.124			
183.7	23.371	0.066	−0.070	0.604	0.133	−0.131	0.918	0.142	−0.149			
201.4	23.594	0.081	−0.087	0.630	0.161	−0.159	0.964	0.167	−0.177			
220.8	23.815	0.098	−0.108	0.661	0.196	−0.192	1.018	0.195	−0.209			
242.1	24.059	0.121	−0.136	0.727	0.240	−0.233	1.072	0.231	−0.251			
265.5	24.381	0.160	−0.187	0.752	0.322	−0.309	1.147	0.292	−0.322			
291.1	24.728	0.214	−0.266	0.822	0.439	−0.410	1.270	0.362	−0.405			
319.2	25.180	0.307	−0.430	0.989	0.655	−0.571	1.477	0.457	−0.522			
349.9	25.599	0.425	−0.709	1.094	1.008	−0.792	1.631	0.594	−0.697			

essentially round there ($0.95 \leqslant A \leqslant 1$) and the cone around the jet has been removed. Thus the apparent rotation of the position angle seen in NGC 4486 is not real. The rotation of the position angle in NGC 4472 first noted by King is confirmed.

There is no apparent difference in the ellipse parameters (i.e., ϵ or position angle) between the various colors in any of the three galaxies. Thus the isophotes are coincident with the isochromes.

The images of NGC 4406 reveal the presence of several dust lanes in the section of the galaxy from 125 to 210 arcsec southeast of the nucleus. The most prominent of these has an absorption of about 5% in the g filter. There is marginal evidence for several areas of absorption within 100 arcsec of the nuclei of NGC 4472 and NGC 4486, but the maximum absorption is less than 1% of the light of the galaxy.

b) Comparison With Previous Studies

A comparison of our photometry with that of Boroson, Thompson, and Shectman (1983) (henceforth referred to as BTS) is extremely encouraging. The upper part of Fig. 1 displays the differences between our measurement of the surface brightness of NGC 4486 in the g filter and that of BTS in the Johnson V filter as a function of semimajor axis. The mean difference is 0.107 mag, with a σ about the mean for the 22 values of A at which the surface brightness was compared over the regime in common, $6.5 \leqslant A \leqslant 157$ arcsec, of 0.016 mag. The difference in our Thuan-Gunn r surface brightness versus their Johnson R values for NGC 4486 is shown in the upper part of Fig. 1. The mean difference is 0.435 mag, with σ about the mean of 0.022 mag over the same radial range. These zero-point differences (0.107 mag and 0.435 mag) are in good agreement with those of the photometric transformation equations between the two systems for objects of the appropriate colors given by Kent (1985). BTS assumed round isophotes. Since the ellipticity of NGC 4486 becomes quite noticeable by $A = 100$ arcsec, this may account for the small relative divergence of $\approx$0.05 mag in our g and r surface-brightness measurements as compared with theirs in the outermost part of the regime of A in common. BTS have given detailed comparisons of their surface photometry with that of numerous previous investigators. More recent CCD photometry of NGC 4486 can be found in Davis *et al.* (1985).

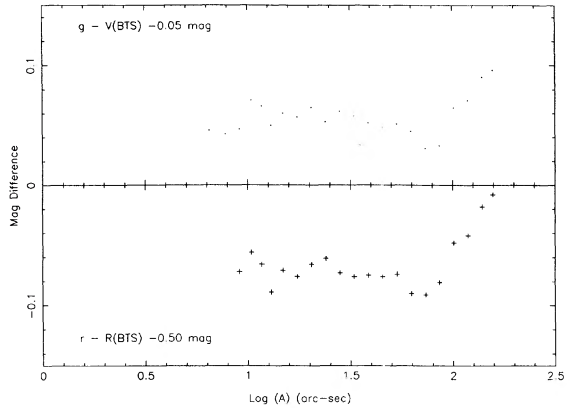

FIG. 1. Difference between the surface brightness of NGC 4486 in the g bandpass determined here and the V surface brightness of BTS is shown as a function of the logarithm of the semimajor axis (A) in the upper part of the figure. In the lower part, the difference between the r surface brightness in the Thuan-Gunn system of NGC 4486 (this paper) and that of BTS using the Johnson R filter is shown.

c) Color Gradients

Color gradients are apparent in all the colors throughout each galaxy, but are quite small, even in the nuclear region. We have derived color gradients by assuming first that the adopted values of the sky are correct, and restricting attention to the part of each galaxy where the uncertainties in the colors are not larger than 0.15 mag. This limits the range in A from 2 to 230 arcsec in NGC 4472 and NGC 4406, and to 184 arcsec in NGC 4486. A maximum color gradient over the same range in A was also derived by assuming that the colors become bluer toward the outer parts of each galaxy and adopting the maximum negative uncertainty in the colors in the outer parts of each galaxy. The nominal and the maximum (blueward) values of the color gradients are listed in Table VI for each galaxy for each of the $(v-g)$, $(g-r)$, and $(g-i)$ colors. The gradients are given as change in color (in units of magnitude) per interval of a factor of 10 in semimajor axis [i.e., per 1 dex in log (A)]. These values are, as is apparent from inspection of Tables III–V, quite small. Transformation equations between the Thuan-Gunn and Johnson photometric systems have been given by Kent (1985) and by Cohen (1985). We can use these to deduce gradients in $B-R$ of between 0.07 and 0.12 mag/dex in A) throughout the range $8 \leqslant A \leqslant \approx 200$ arcsec in these three elliptical galaxies. This is in good agreement with the values found by BTS for the color gradient in $B-R$ of 0.09 to 0.14 mag/dex in A in the inner part of NGC 4486.

Table VI demonstrates that the color gradients are small throughout the entirety of these three Virgo ellipticals. Only a limited sample of the large body of earlier photographic studies of these galaxies, including for example that of Carter and Dixon (1978), derived such small color gradients. Errors in determination of the sky undoubtedly played a more substantial role than was realized at the time in the many analyses in which the existence of large color gradients was claimed (for example, that of Strom *et al.* 1981).

We attempt to demonstrate that small color gradients can easily be produced by metallicity gradients within a purely old population with a normal initial-mass function. From the photometric data of Hamuy (1984) for the galactic globular clusters, their reddenings from Harris and Racine (1979), and their metallicities from Zinn and West (1984), we derive $\delta(B-R) = 0.28$ mag for a factor of 10 change in metallicity. There is a correction factor in extrapolating these results to the more metal-rich population of NGC 4486 such that a smaller color change is expected for a given metallicity change, but we ignore it to first order. We thus find that a metallicity gradient of $\approx$0.5 dex in metallicity /1 dex

TABLE VI. Color gradients in three Virgo elliptical galaxies.

	M87	NGC 4472 (Δ mag/Δ log A = 1.0)	NGC 4406
$v-g$	0.13	0.15	0.07
$v-g$ (max)	0.17	0.26	0.20
$g-r$	0.04	0.04	0.04
$g-r$ (max)	0.06	0.04	0.08
$g-i$	0.05	0.05	0.09
$g-i$ (max)	0.10	0.12	0.16

in log (A) would produce the observed color gradients in the outer parts of the Virgo ellipticals. The metallicity gradient in the disk of the Milky Way determined by Janes (1979), when expressed in these units, is about three times larger than that which we determine for NGC 4486. This leaves ample room for the correction factor we choose to neglect, and substantiates our assertion that the radial color gradients in the Virgo ellipticals can arise purely from radial metallicity gradients.

V. SUMMARY

CCD images using the 4-Shooter on the Hale telescope at Palomar Observatory have been obtained for the luminous Virgo ellipticals NGC 4486, NGC 4472, and NGC 4406 in the v, g, r, and i filters of the Thuan-Gunn system. The large format of the frames (square 9 arcsec on a side) allows accurate surface photometry and galaxy colors to be determined. The frames were fit by ellipses whose ellipticity and position angle were allowed to vary as a function of semimajor axis.

The major results of this work are twofold. First, for each galaxy there is no systematic difference larger than the errors between the parameters of the ellipse fits among the four colors. Thus the isophotes and isochromes coincide. More importantly, the color gradients in the three galaxies extending over the regime $2 \leqslant A \leqslant \approx 400$ arcsec, are small, of order 0.1 mag/factor of 10 in A. These color gradients are probably a manifestation of radial metallicity gradients. A forthcoming publication will compare the properties of the globular cluster systems in each of the three galaxies to those of the underlying galaxies as given here.

REFERENCES

Boroson, T. A., Thompson, I. B., and Shectman, S. A. (1983). Astron. J. **88**, 1707.

Carter, D., and Dixon, K. L. (1978). Astron. J. **83**, 574.

Cohen, J. G. (1985). Astron. J. **90**, 2254.

Davis, L. E., Cawson, M., Davies, R. L., and Illingworth, G. (1985). Astron. J. **90**, 169.

de Vaucouleurs, G., and Nieto, J. L. (1978). Astrophys. J. **220**, 449.

Ford, H. C., and Butcher, H. (1979). Astrophys. J. Suppl. **41**, 147.

Gunn, J. E., Carr, M., Chang, J., Danielson, G. E., Lorenz, E. O., Lucinio, R., Nenow, V. E., Smith, O. J., Westphal, J. A., and Zimmerman, B. A. (1984). Bull. Am. Astron. Soc. **16**, 447.

Hamuy, M. (1984). Astron. Astrophys. Suppl. **57**, 91.

Harris, W. E., and Racine, R. (1979). Annu. Rev. Astron. Astrophys. **17**, 241.

Janes, K. A. (1979). Astrophys. J. Suppl. **39**, 135.

Kent, S. M. (1983). Astrophys. J. **266**, 562.

Kent, S. M. (1985). Publ. Astron. Soc. Pac. **97**, 165.

King, I. R. (1978). Astrophys. J. **222**, 1.

Schmidt, M., Schneider, D., and Gunn, J. E. (1986). Astrophys. J. **306**, 411.

Strom, S. E., Forte, J. C., Harris, W. E., Strom, K. M., Wells, D. C., and Smith, M. G. (1981). Astrophys. J. **245**, 416.

Thuan, T. X., and Gunn, J. E. (1976). Publ. Astron. Soc. Pac. **88**, 543.

Zinn, R., and West, M. J. (1984). Astrophys. J. Suppl. **55**, 45.